analytical chemistry

Article

pubs.acs.org/ac

# Multiphoton Excitation of Upconverting Nanoparticles in Pulsed Regime

Jose Hodak,[†] Zhijun Chen,[‡] Si Wu,[‡] and Roberto Etchenique*[,†]

[†]Departamento de Química Inorgánica, Analítica y Química Física, INQUIMAE, Facultad de Ciencias Exactas y Naturales, Universidad de Buenos Aires, Ciudad Universitaria Pabellón 2, AR1428EHA Buenos Aires, Argentina

[‡]Max Planck Institute for Polymer Research, Ackermannweg 10, 55128 Mainz, Germany

Supporting Information

**ABSTRACT:** Upconverting nanoparticles (UCNPs) present emission in the visible region upon irradiation with NIR light through a multiphoton mechanism. However, the long characteristic time of their emission has prevented the use of this kind of entities as multiphoton probes. We present a study on the use of erbium-containing UCNPs under pulsed excitation, showing that both the power density and the duration of the excitation pulse are key factors to understand the emission behavior. By adjusting power and excitation rate, we can obtain typical multiphoton *z*-axis focal exclusive excitation. These findings open the possibility of using UCNPs as probes for controlled localization of uncaging and imaging with multiphoton *z*-axis sectioning. We show that this can be achieved even at power densities several orders of magnitude lower than traditional multiphoton microscopies.

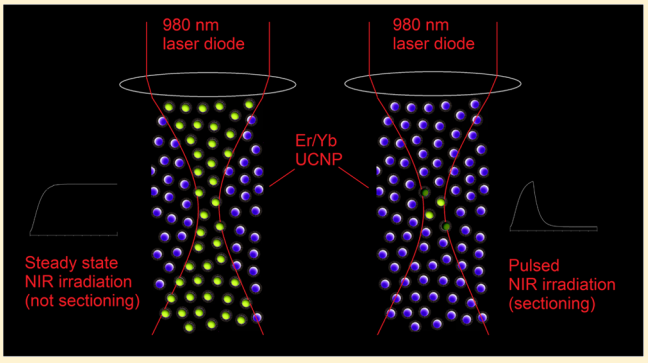


Since Denk reported the first two-photon scanning fluorescence microscope,[1] imaging techniques based in multiphoton (or nonlinear) excitation grew in explosive form. Multiphoton excitation presents two main advantages over usual linear luminescence: a lower scattering due to the antiStokes shift of the emission and an intrinsic sectioning capacity due to the dependence of the emission with higher powers of the excitation power density. The latter characteristic is the basis for microscopy techniques based on two-photon absorption both in imaging[2−4] and uncaging procedures.[5−8]

Two photon (2P) absorption is an excitation pathway in which two photons of a given energy are absorbed quasi-simultaneously to reach an excited state that usually only can be populated with light of about twice that energy. For this absorption to take place, a very high instantaneous power density has to be achieved, in order to allow the probe to absorb more than one photon in about $10^{-16}$ s.[9] Once the excited state is populated, the photophysics and photochemistry of the process follow the usual decay pathways. In similar ways more than two photons can be absorbed. Figure 1a shows a state diagram that illustrates this mechanism.

In order to have such a high photon density, instantaneous power in the range of $10^{13}$ W/cm$^2$ is required. This is achieved through femtosecond lasers, which permit to obtain such an enormous instantaneous power without damaging the sample due to overheating. Femtosecond lasers (usually Ti-Sapphire) are expensive and hard to maintain, and these facts are at the present time the main drawback of the 2P techniques. Two alternatives were proposed to reduce the needed power density of 2P excitation: increasing a nonlinear cross section and chemical-2P approaches. Most probes present a very low 2P absorption cross section, on the order of 1−200 GM (1 Goeppert−Mayer = $10^{50}$ cm$^4$ s), that led to low emission even at very high excitation fluxes. By increasing this absorption it is possible to reduce the power of light needed for imaging. This strategy, combined with engineering of new probes, has been used successfully.[10,11] The second strategy implies the use of a chemically active probe that is inactive until a first photon triggers the molecule. A second photon can now promote the excited state population that led to emission[12] or uncaging (photolysis) of a desired molecule.[13] This chemical-2P mechanism allow the use of low power CW lasers (i.e., laser diodes), but there are some drawbacks to this approach. Both photons are in the UV or visible range instead of NIR, implying higher scattering and no reversible probe capable of reinactivating after irradiation has yet to be designed and synthesized.

A new generation of probes based on luminescent nanoparticles was devised in the last years.[14,15] Being nanometer sized objects rather than molecules, their stability against photobleaching is very good, while its size is small enough to be used and delivered to target specimens to be imaged. Among them, certain lantanides-doped phosphors can sequentially absorb several low energy (NIR) photons to populate high

**Received:** November 26, 2015
**Accepted:** December 24, 2015
**Published:** December 24, 2015





DOI: 10.1021/acs.analchem.5b04485
*Anal. Chem.* 2016, 88, 1468−1475

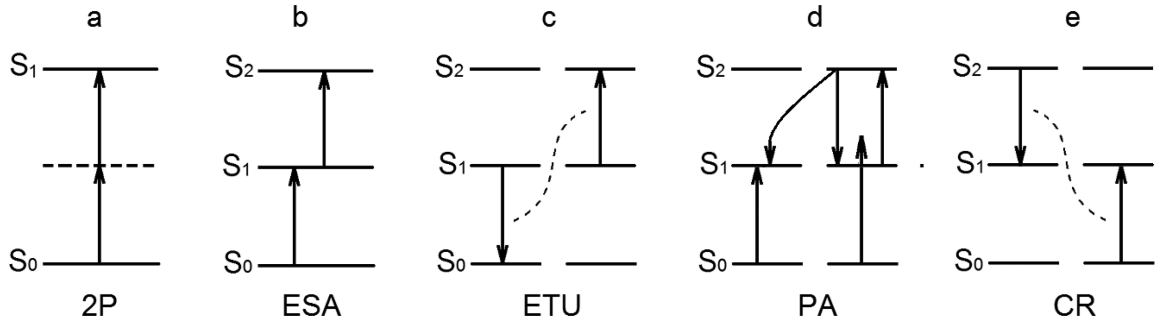


**Figure 1.** Scheme of 2-photon absorption compared with some mechanisms involved in upconversion processes: (a) two photon absorption (2P), depicting the virtual state between S1 and S2; (b) excited state absorption (ESA), showing the real intermediate state; (c) energy transfer upconversion (ETU); (d) photon avalanche mechanism (PA); (e) cross relaxation (CR).

energy excited states from which they emit visible photons in a process called upconversion.[16−18] Thus, this kind of probes are generally addressed as upconverting nanoparticles (UCNPs).

The mechanism by which UCNPs operates is quite different from that for the traditional 2P absorption. In the latter excitation mechanism there is no real resonant excited state between the ground level and the state from which the emission occurs (Figure 1a). Conversely, in the upconversion process one or more long-lived intermediate excited states acts as energy reservoirs. From these intermediate states, subsequent one photon excitations and energy transfer processes populate a manifold of higher energy states. Some of the usual mechanisms that take place in the upconversion process are depicted in Figure 1.

The presence of long-lived real intermediate states implies that low energy excitation can be used to achieve upconversion. Typical laser diode sources are sufficient to activate the multiphoton conversion, allowing anti-Stokes luminescence that is becoming widely applied in security printing industries, mainly counterfeit detection (i.e., Russian and Chinese banknotes). The NIR excitation (typically 980 nm) and its associated high penetration and low scattering in biological tissues offer a good way to illuminate deep regions. Recently, the combination of Ru-based caged compounds, capable to photorelease biomolecules[7,19−22] with UCNP showed that it is possible to release a drug by means of low energy NIR photons with excellent performance.[23−25]

However, one of the main advantages of multiphoton excitation, the capability of sectioning, was not achieved using UCNPs. Their long emission characteristic times ($\tau \sim 200\ \mu s$) make difficult the use of typical Ti-Sapphire lasers and prevent the use of descanned confocal microscopes. Ingenious deconvolution methods have been devised to circumvent this problem.[26]

Any scanning microscopy technique necessarily irradiates each point of the sample during a very short time, which can be much shorter than the characteristic time of a typical phosphor. Unfortunately, there are not many studies regarding lanthanide phosphors and UCNP behavior in a pulsed regime. These kind of studies are necessary to design a useful method for that takes advantage of UCNP intrinsic multiphoton sectioning potential. We present a theoretical and experimental study of UCNP excitation under a pulsed regime, showing that the excitation time can be exchanged for power density, allowing real sectioning in the *z*-axis, and opening a new perspective in the use of upconverting probes as tools for new inexpensive 2P microscopies.

## EXPERIMENTAL SECTION

All reagents were commercially available and used as received. The Er-containing UCNPs (core = $NaYF_4$−2 mol % $Er^{3+}$−30 mol % $Yb^{3+}$; shell = $NaYF_4$) and phosphors were synthesized as published[24] or obtained commercially from Shanghai Keyan Phosphor Technology Co., Ltd. A transmission electron microscope image of the used UCNPs is given as Supporting Information.

The UV−vis spectra were taken with an Ocean Optics CHEM2000 diode-array spectrometer. A TO-18 (5.6 mm diameter, LCU985041A or similar), 50 mW, 980 nm laser diode was used to excite the upconversion emission of the used phosphors. The device were mounted onto an Al block to prevent heating and pulsed by means of a CMOS buffer. An ad-hoc power supply, controlled from a PC-computer through a Keithley DAS20 acquisition card was used to control the instantaneous power of the pulses. The pulse timing was determined through the parallel port using a software written in QuickBasic 4.5 and Assembler 80286. The used circuit is depicted as Supporting Information.

The laser diode was collimated using a 7 mm focal distance lens and further focused through 10× $N_A$ = 0.25 or 20× $N_A$ = 0.40 microscope objectives. A dichroic mirror prior to the objective path allowed one to measure the visible emission without interference of the NIR reflection on the sample. Two interference short pass filters at 750 nm were used to block the remanent NIR radiation. The emission was focused onto an amplified photodiode (Edmund Optics PDA100A) or directly to the Ocean Optics fiber optics spectrometer. The traces of the time-resolved emission were acquired with a Hantek 6022BE digital oscilloscope.

## RESULTS AND DISCUSSION

Figure 2 shows the emission spectra of Er-containing UCNP under excitation with 980 nm at different intensities, using a collimated CW laser diode. The four stronger emission bands appear at 660, 550, 525, and 411 nm. These transitions correspond to $^4F_{9/2}$−$^4I_{15/2}$, $^4S_{3/2}$−$^4I_{15/2}$, $^2H_{11/2}$−$^4I_{15/2}$, and $^2H_{9/2}$−$^4I_{15/2}$, respectively,[27] being the first two responsible for 90% of the total emission.

A log−log plot of 660 and 550 nm emission against the excitation emission (Figure 2, insets) clearly show slopes greater than 1, indicating a multiphoton pathway. However, in the conditions of the experiment, both slopes are lower than 2 (which corresponds to a full two-photon excitation). When the power density of the excitation was increased by focusing the light into a narrower beam, both slopes decreased approaching


DOI: 10.1021/acs.analchem.5b04485
*Anal. Chem.* 2016, 88, 1468−1475

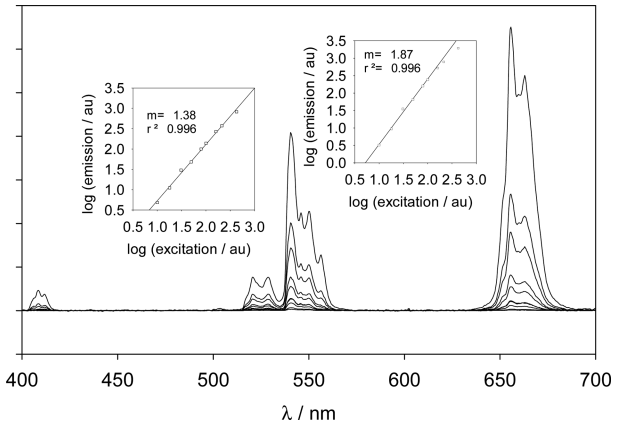


**Figure 2.** Emission spectra of for a 5% w/w suspension of Er-containing UCNPs in cyclohexane under excitation at 980 nm at several excitation intensities. Left inset: log−log plot of the 550 nm band ($^4S_{3/2}$−$^4I_{15/2}$) and 660 nm band ($^4F_{9/2}$−$^4I_{15/2}$) and best linear fit indicating power of dependence. Note that the three higher measurements on the 660 nm band deviated from the linear fitting.

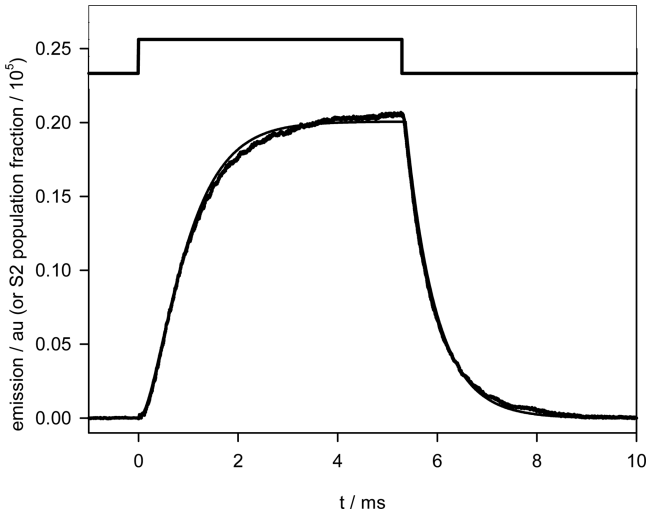


**Figure 3.** Time dependence of the emission of the 550 nm ($^4S_{3/2}$−$^4I_{15/2}$) band under a pulsed excitation at 980 nm for Er-containing UCNPs. Top line: excitation pulse. Bottom line: experimental values and its fitting to a theoretical model (see text).

unity. This behavior is characteristic of a saturation process in which the population of the intermediate states, that "store" the first photon before another one promotes the NP to its final emissive state, is no longer negligible. When saturation of the intermediate state occurs, single photons can excite NP from the rather occupied intermediate state to the final emissive state; therefore, luminescence becomes a quasi-one photon process, eliminating the characteristic 2P quadratic dependence on the excitation power. As this nonlinear dependence between excitation and emission is a mandatory condition to achieve *z*-axis sectioning, saturation of the UCNP constitute an important obstacle that must be surmounted.

Lanthanide-doped UCNPs present long-lived states, as expected for their mechanism of energy conversion. The exact time dependence characteristics of their emission vary depending on the aggregation state. Solid particle-like aggregates deposited into substrates tend to yield longer emission lifetimes, while NP sized phosphors in colloidal suspensions present somewhat shorter response. Figure 3 (dots) shows a typical dependence on the emission during a 980 nm excitation pulse.

While the decay is monoexponential with a characteristic time $\tau$ = 602 $\mu$s, the rise of the curve is more complex. The initial onset indicates a rather slow mechanism of population of the intermediate state, needed to absorb new photons to reach the final emissive state. Gamelin and Gudel[28] have described a three-states model to simulate this behavior. Although ESA and ETU mechanisms are probably present in our phosphors, and several different multiphoton pathways are surely involved in their photophysics, we have been able to describe the key characteristics of our system by means of a simplified model. It is important to keep in mind that upconversion is a rather complex process, in which the emissive states can be reached by many different pathways. As each pathway involves several accumulation and decay steps that have different rates and can be more or less populated, usually the emission power dependence on excitation is not an integer (as would correspond to neat 2, 3, 4, etc. photon processes) but fractional. We have chosen two of the typical emission bands of the Er-containing nanoparticles, which have been profusely studied and present a quite simple near-2-photon behavior. The 550 nm band ($^4S_{3/2}$−$^4I_{15/2}$) presents higher intensity at low excitation power and is more suitable for kinetic studies. The 660 nm band ($^4F_{9/2}$−$^4I_{15/2}$), on the other hand, has an emission intensity that scales almost as a pure 2-photon process and is better to investigate the imaging applications. Any added complexity can be useful to match even more carefully the experimental data but does not change the main panorama. We have used a more elaborated model to allow a comparison with traditional 2P excitation, which is given as Supporting Information. In order to gain some insight about the factors that determine the emission performance of the phosphor nanoparticles, simulations were carried out by means of a model represented by the following equations system:

$$\frac{dN_0}{dt} = -GN_0 + k_1N_1 + k_2N_2 \quad (1)$$

$$\frac{dN_1}{dt} = GN_0 - k_1N_1 - EN_1 \quad (2)$$

$$\frac{dN_2}{dt} = EN_1 - k_2N_2 \quad (3)$$

where $N_0$, $N_1$, and $N_2$ are the populations of the ground ($S_0$), intermediate ($S_1$) and emissive ($S_2$) states, $G$ the ground state excitation rate constant, $k_1$ the decay constant from the intermediate state; $k_2$ the decay constant from the emissive state and $E$ is the ESA excited state excitation rate constant, by which a further photon can populate the $S_2$ state from $S_1$. In order to simplify the model, no decay path from $S_2$ to $S_1$ was taken into account, neither any nonradiative mechanisms, although they are obviously present. The respective rate constants are included in $k_2$ and $k_1$. For our purposes absolute measurements of upconversion quantum yield were not essential. Instead, we choose to fit the parameters of our simplified model to the experimental data to extract the rates. From these fits, we first found the following set of parameters: $G$ = 30 $s^{-1}$; $E$ = 8.2 × $10^{-3}$ $s^{-1}$, $k_1$ = 2.16 × $10^3$ $s^{-1}$; $k_2$ = 1.66 × $10^3$ $s^{-1}$. As $k_2$ can be measured directly from the decay after the pulse excitation, it was fixed as constant. The value of $G$ and $E$ include the excitation intensity and are related to the initial


DOI: 10.1021/acs.analchem.5b04485
*Anal. Chem.* 2016, 88, 1468−1475

population of ground state $N_0$. We have fixed $N_0$ = 10 000, but other combinations of $N_0$, $G$, and $E$ yield similar results.

Figure 4 shows the experimental data and the corresponding simulation of the phosphor response using our model, for the previously fitted parameters and pulse widths of 330, 660, 1320, 2650, and 5300 $\mu$s. The $y$-axis represents the fraction of populated emissive excited states or the corresponding emission intensity (in arbitrary units). It is important to remark that even short pulses will decay with the long characteristic time of lanthanide phosphorescence, and therefore the probes will present low photon flux under those conditions.

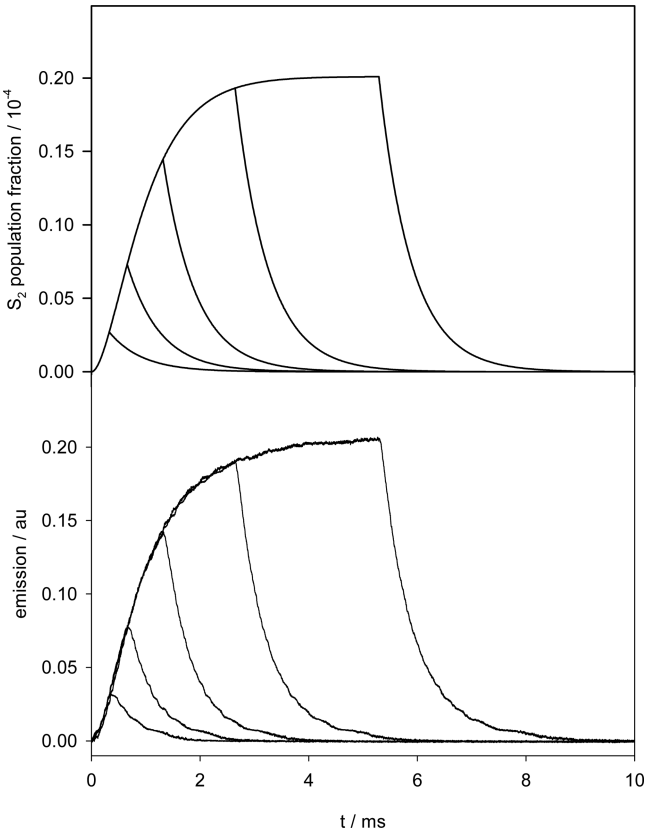


**Figure 4.** (Top) Fraction of populated emissive state for a simplified upconversion mechanism, with $G$ = 30 $s^{-1}$; $E$ = 8.2 × $10^{-3}$ $s^{-1}$, $k_1$ = 2.16 × $10^3$ $s^{-1}$; $k_2$ = 1.66 × $10^3$ $s^{-1}$. (Bottom) Experimental emission. The excitation is given as pulses of 330, 660, 1320, 2650, and 5300 $\mu$s length. ($c_{NP}$ = 15 mg/mL, $I_{exc}$ = 10 W/$cm^2$).

The expected dependence of the emission with the excitation intensity can also be calculated with the same simplified model. For a 2P process with a long enough excitation pulse in order to achieve the emission steady state, a quadratic response is expected. Figure 5a shows this behavior when the population fraction of $S_1$ and $S_2$ remain low. However, at higher photon absorption rates, the intermediate state population increases and the emission-excitation dependence will be intermediate between linear and quadratic as shown in the previous experiment (Figure 2b).

Notably, when the excitation pulse width is much shorter than the characteristic time of the UCNPs, almost complete equivalence can be found between power dependence and pulse length dependence. Figure 6 (solid lines) shows the emission for pulses of 100 $\mu$s width, at relative excitation

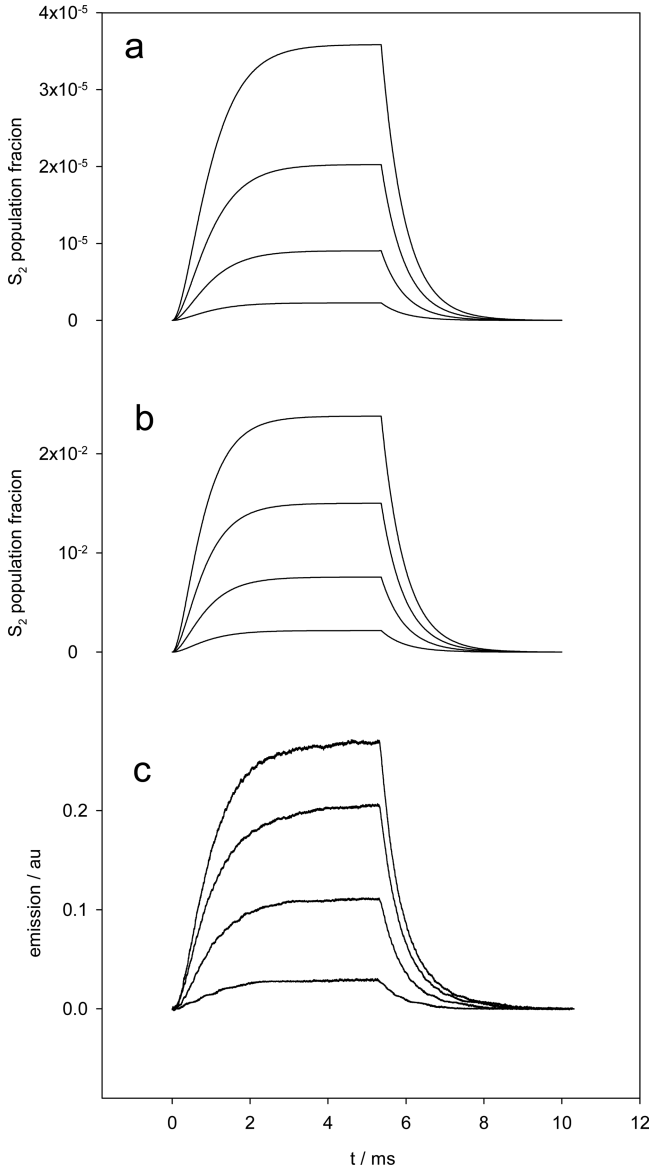


**Figure 5.** Fraction of populated emissive state for simplified upconversion mechanism, with $G$ = $I_{exc}$ × 0.3 $s^{-1}$; $E$ = $I_{exc}$ × 8.2 × $10^{-5}$ $s^{-1}$, $k_1$ = 2.16 × $10^3$ $s^{-1}$; $k_2$ = 1.66 × $10^3$ $s^{-1}$. (a) $I_{exc}$ varies from 1 to 4 at linear steps, showing quadratic response in the steady state. (b) $I_{exc}$ varies from 3 × $10^4$ to 12 × $10^4$ at linear steps, showing lower than quadratic dependence due to intermediate state saturation. (c) Experimental emission in saturation conditions similar to part b ($c_{NP}$ = 15 mg/mL, $I_{exc}$ = 500 W/$cm^2$).

intensities of 1, 2, 3, and 4. The dotted lines show the results for the maximum excitation intensity, while changing the pulse width between 25 and 100 $\mu$s. Both cases are almost indistinguishable, showing the quadratic response on the integrated emission (see inset) and complete correspondence between pulse time and intensity.

In the case that the pulses are not much shorter than the characteristic times of the upconversion process, this equivalence does not hold and the time-dependent emission shapes vary depending on power density and pulse length. However, the total amount of emission shows the same dependence on the overall average excitation, regardless of the method (variable density power or variable pulse length) used for modulation of the excitation. These results agree completely


DOI: 10.1021/acs.analchem.5b04485
Anal. Chem. 2016, 88, 1468−1475

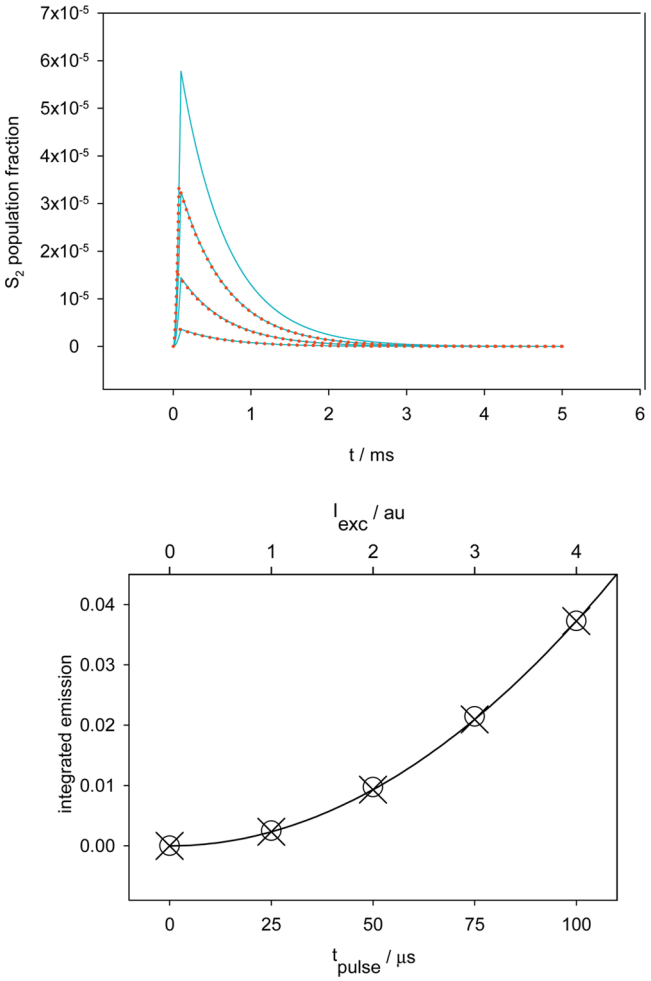


**Figure 6.** (Top) Fraction of populated emissive state for simplified upconversion mechanism, with $G = I_{exc} \times 3\ s^{-1}$; $E = I_{exc} \times 8.2 \times 10^{-3}\ s^{-1}$, $k_1 = 2.16 \times 10^3\ s^{-1}$; $k_2 = 1.66 \times 10^3\ s^{-1}$. Cyan solid lines: pulse duration, 100 $\mu$s; intensities $I_{exc}$ = 1, 2, 3, and 4 arbitrary units. Red dotted lines: $I_{exc}$ = 4 au; pulse duration, 25, 50, and 75 $\mu$s. The quadratic response and the total equivalence of increasing power and pulse duration are apparent. Bottom: ○ emission integration of cyan solid lines; × emission integration of red dotted lines.

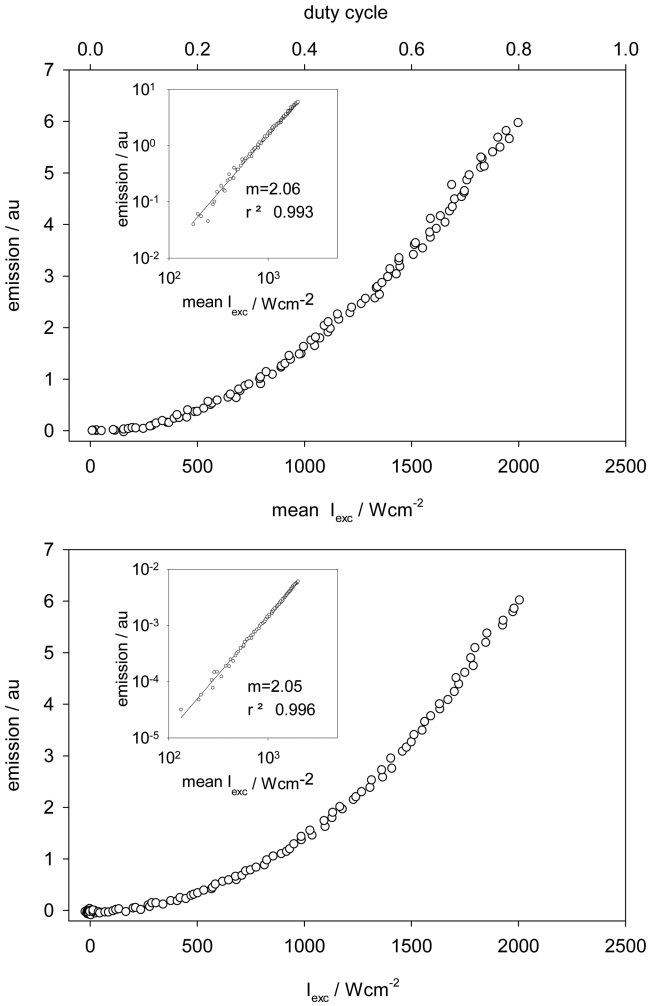


**Figure 7.** (Top) Integrated emission of the 660 nm $^4F_{9/2}$–$^4I_{15/2}$ band under pulsed (1000 Hz) excitation. The duty cycle of the square wave varies between 0 and 1, while the power is kept constant at 2000 W/cm$^2$. Note the quadratic response of the emission. The log–log plot (inset) indicates a slope of 2.06, corresponding to an effective 2-photon process. (Bottom) Integrated emission of the 660 nm $^4F_{9/2}$–$^4I_{15/2}$ band under continuous excitation power that varies from 0 to 2000 W/cm$^2$.

with the experimental findings. Figure 7 (top) shows the dependence of the emission intensity for the 660 nm $^4F_{9/2}$–$^4I_{15/2}$ transition with the pulse duty cycle ($f$ = 1000 Hz) at a constant excitation power density. In this way, the average power is varied from 0 to 2000 W/cm$^2$. On the other hand, Figure 7 (bottom) shows the dependence of the emission intensity for the same transition at steady excitation at variable power between 0 and 2000 W/cm$^2$. Note the correspondence of both methods of varying average excitation power.

At low level overall excitation, due to either short pulses or low power density, the slope approaches 2, indicating full two-photon behavior (see inset in Figure 7). At higher excitation this slope diminishes toward a linear process, as predicted by the model, and later even shows a less than unity slope (see the Supporting Information).

These facts suggest the strategy to follow in order to get the sectioning capabilities of the multiphoton excitation using UCNPs. The overall excitation intensity on the probe (power density times pulse duration) must be low enough to prevent saturation of the intermediate states. This saturation and reduction of nonlinearity between emission and excitation is the main problem that prevents UCNPs as 2P probes. Some authors have reported the failure to obtain real focal sectioning using continuous excitation.[29,30] The high power density needed to obtain an adequate signal-to-noise ratio prevents the probes to present nonlinear emission dependence near the focal point. However, as for imaging techniques each pixel is illuminated just a brief fraction of the total frame time, pulsed excitation instead of CW must be investigated. For an image of 0.3 megapixel (640 × 480) to be taken in 1 s, each pixel is excited just about 3.2 $\mu$s, a hundred times shorter than the characteristic luminescence time. Therefore, it is possible to keep the total amount of light in an adequate level by rapidly scanning the frame while collecting the emission in a parallel integrative way. It is important to see that the emission photon collection cannot be done using the usual procedure of sequential descanning, given that the long characteristic times of UCNP luminescence would imply to wait several milliseconds per pixel, even though the excitation lays in the microseconds. The easiest alternative is obviously a parallel


DOI: 10.1021/acs.analchem.5b04485
Anal. Chem. 2016, 88, 1468–1475

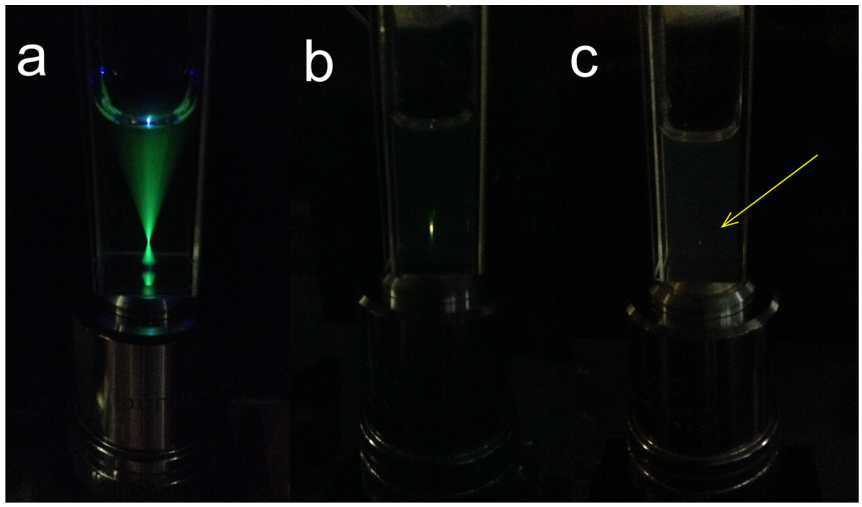


**Figure 8.** Comparison between 1-photon and 2-photon excitation: (a) a solution of the fluorescent dye Pyranine, excited in 1P regime with a 450 nm laser through a 20× $N_A$ = 0.4 microscope objective; (b) a suspension of 15 g/L Er-Yb UCNPs in cyclohexane excited by means of a focused 980 nm beam in continuous regime (2 kW/cm$^2$). (c) The same suspension excited in a low duty cycle pulsed mode (50 $\mu$s on, 4950 $\mu$s off) in order to avoid saturation of the intermediate states, recovering the quadratic dependence and the sectioning capabilities. The visible dot size is below the camera image capabilities (<15 $\mu$m diameter).

detection scheme using a CCD camera, in which the pixels can be detected in their proper place in an integrating frame in the millisecond range.

As a proof of principle, Figure 8 shows the comparison between 1P excitation and 2P upconversion excitation. Figure 8a depicts the typical emission bicone generated by 1P excitation of a fluorophore (Pyranine) focused through a 20× $N_A$ = 0.4 objective. In parts b and c, a suspension of UCNPs excited at 980 nm is focused through the same objective in continuous and pulsed mode. While Figure 8b shows some biconical emission due to saturation of the intermediate state, the cuvette under low duty cycle pulsed excitation (Figure 8c) shows a typical "focal dot emission" indicating that sectioning is possible in these conditions.

As a further test of the capabilities of this technique we have built a simple scanning microscope with detection using a CCD webcam as parallel detector. A collimated beam provinient from the 980 nm laser diode was directed using two galvanometer mirrors and two F:2F:F relay telescopes onto the objective (10×, $N_A$ = 0.4). The mirrors allow the focused dot to be scanned onto the specimen in 0.5 s (480 lines). At this speed, each pixel in the camera is illuminated during 0.5 s/(480 × 640 pixels) = 1.62 $\mu$s, being well within the low duty cycle needed for sectioning. (In fact, as the focusing is not perfect, the specimen presents high light dispersion and emissive zones can be bigger than 1 pixel wide, the real time that the beam irradiates an independent area of the specimen could be between 2 and 10 $\mu$s).

Even for this very crude scanning microscope, the difference between direct upconversion and sectioning scanning upconversion imaging is dramatic. Figure 9 shows five images at $z$ depths differing 25 $\mu$m each. The images at the left were taken with a nonfocused 980 nm IR beam. The images at the right were obtained by focused scanning, allowing sectioning upconversion. The camera gain was regulated to get similar amounts of total light. Note the higher brightness of the out of focus regions (left, bottom) compared to that for the corresponding images at the right.

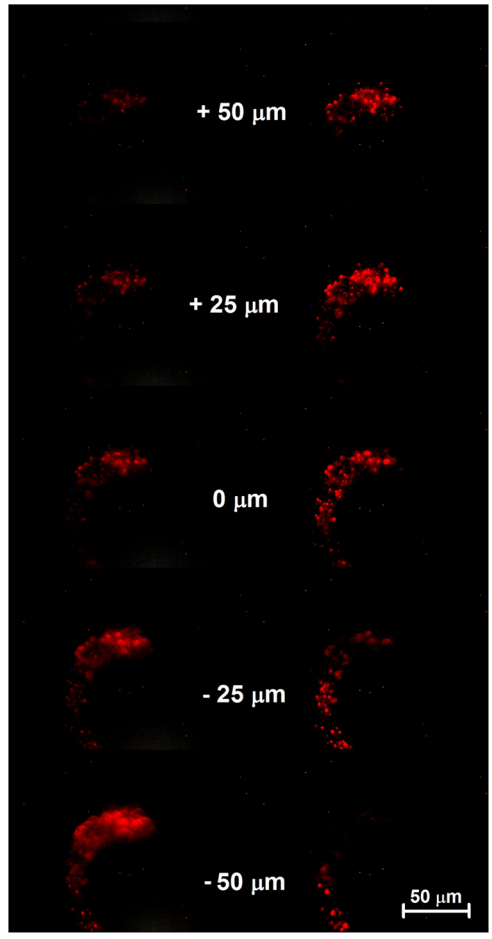


**Figure 9.** Comparison between direct and scanned upconversion imaging. (Left) A nylon specimen stained with UCNPs imaged through a 10×, $N_A$ = 0.4 objective under direct illumination (980 nm, 10 W/cm$^2$). (Right) The same specimen imaged through scanning (980 nm, 20 kW/cm$^2$, 640 × 480 pixels, 0.5 s exposition). Note the z-sectioning of the images at the right panel.



DOI: 10.1021/acs.analchem.5b04485
*Anal. Chem.* 2016, 88, 1468−1475

It is important to remark that although they are two different processes, the equations governing the sectioning capabilities of pulsed upconversion imaging are the same that traditional 2P imaging using Ti-sapphire femtosecond lasers. This fact strongly suggests that the theoretical limit in $z$-sectioning is as good as in typical 2P microscopies.

The capability of using a low power laser diode instead of a extremely high instantaneous power femtosecond laser indicates that the effective cross section for 2P absorption of the UCNP appears as very high. Strictly speaking, the initial absorption in UCNPs is a simple 1-photon process. It is the inner accumulation mechanism that allow this initial 1P process to be capable to populate higher states that emit in the visible region. As a comparison, it is possible to calculate the 2-photon cross section that an emitter should have to convert the same proportion of IR photons into visible emission that the UCNPs in sectioning regime and using the same excitation power density. Using a somewhat complex model it is possible to estimate that an average $I_{exc}$ = 42 W/cm$^2$ is capable to populate the excited state of the UCNP to a fraction $x_2 = 10^{-4}$, allowing an emission efficiency of $2.37 \times 10^{-3}$, equivalent to a flux of about $5 \times 10^{17}$ photons/s. For obtaining the same flux through a typical 2P process and using the same excitation $I_{exc}$, the fluorophore should have an effective cross section of $7.6 \times 10^8$ GM (1 Goeppert Mayer = $10^{-50}$ cm$^4$ s photon$^{-1}$). By way of comparison, a typical fluorescent molecule active in the 2P regime ranges between 1 and 200 GM.[31] A CdTe or CDSe nanoparticle can be as high as $5 \times 10^4$ GM.[32] On the other hand, the price that has to be paid for this enhancement is a slow emission rate. Because of this, while the UCNPs excited states occupancy in the referred conditions is about $10^{-4}$, the corresponding occupancy for a true 2P system is as low as $x_2 = 1.7 \times 10^{-10}$. A more detailed description of this comparison is given as Supporting Information.

This enormous effective 2P cross section of the UCNP is an alternative way to indicate the rather low energy densities that can be used to excitate the multiphoton emissive states.

This strategy could also be used for local uncaging of drugs using the sectioning capabilities of the multiphoton excitation. The possibility to use a rather low instantaneous density power (~20 kW/cm$^2$) as compared with typical 2-photon techniques based in the absorption of Ti-sapphire femtosecond pulses allow the irradiation of biological tissues with no damage at very low cost and allowing a precise $z$-directioning. Together with the recent advances in upconversion-aided phototriggering,[33] the sectioning capability on UCNPs in pulsed regime can be the starting point of real 3D photodynamic therapy.

## CONCLUSIONS

We have showed that lanthanide-doped UCNPs and phosphors can be used as probes in the pulsed excitation regime. Choosing adequately the parameters of the excitation, mainly instantaneous power density, pulse duration, and duty cycle, it is possible to recover the full 2P quadratic emission vs excitation dependence, which is usually obscured due to saturation of intermediate states.

We have characterized the pulsed behavior of Er-containing phosphors and UCNPs, showing that changes in instantaneous power are completely equivalent to changes in pulse length, being interchangeable parameters in order to achieve full 2P behavior. This strategy allowed us to obtain $z$-axis sectioning capabilities by means of preventing saturation through low duty cycle pulsed excitation.

The power needed to elicit this response is many orders of magnitude lower than in the typical 2P excitation and can be obtained with inexpensive laser diodes instead of Ti-sapphire femtosecond pulsed lasers. The control of the involved pulses is also simple, in the range of the micro/miliseconds, allowing the use of very simple electronics. Further work in custom imaging and uncaging microscopy techniques using sequential excitation and parallel detection are under development.

## ASSOCIATED CONTENT

### Supporting Information

The Supporting Information is available free of charge on the ACS Publications website at DOI: 10.1021/acs.analchem.5b04485.

Diagram of the power supply, TEM image of the UCNP, excitation−emission plots covering several orders of magnitude on power density, and details on the calculation of the cross section (PDF)

## AUTHOR INFORMATION

### Corresponding Author

*E-mail: rober@qi.fcen.uba.ar.

### Notes

The authors declare no competing financial interest.

## ACKNOWLEDGMENTS

This research was supported by the National Agency for Science and Technology Promotion, CONICET, and the UBACyT and Deutsche Forschungsgemeinschaft (DFG, WU 787/2-1) . R.E. and J.H.H. are members of CONICET. Z.C. was supported by the CSC program.

## REFERENCES

(1) Denk, W.; Strickler, J. H.; Webb, W. W. *Science* **1990**, *248*, 73−76.
(2) Nikolenko, V.; Poskanzer, K. E.; Yuste, R. *Nat. Methods* **2007**, *4*, 943−950.
(3) Svoboda, K.; Yasuda, R. *Neuron* **2006**, *50*, 823−839.
(4) Chaigneau, E.; Oheim, M.; Audinat, E.; Charpak, S. *Proc. Natl. Acad. Sci. U. S. A.* **2003**, *100*, 13081−13086.
(5) Judkewitz, B.; Roth, A.; Hausser, M. *Neuron* **2006**, *50*, 180−183.
(6) Donato, L.; Mourot, A.; Davenport, C. M.; Herbivo, C.; Warther, D.; Léonard, J.; Bolze, F.; Nicoud, J.-F.; Kramer, R. H.; Goeldner, M.; Specht, A. *Angew. Chem., Int. Ed.* **2012**, *51*, 1840−1843.
(7) Fino, E.; Araya, R.; Peterka, D. S.; Salierno, M.; Etchenique, R.; Yuste, R. *Front. Neural Circuits* **2009**, *3*, 1−9.
(8) Araya, R.; Andino-Pavlovsky, V.; Yuste, R.; Etchenique, R. *ACS Chem. Neurosci.* **2013**, *4*, 1163−1167.
(9) Diaspro, a.; Chirico, g.; Collini, m. *Q. Rev. Biophys.* **2005**, *38* (2), 97−166.
(10) Spangenberg, A.; Malval, J.-P.; Akdas-Kilig, H.; Fillaut, J.-L.; Stehlin, F.; Hobeika, N.; Morlet-Savary, F.; Soppera, O. *Macromolecules* **2012**, *45*, 1262−1269.
(11) Martineau, C.; Lemercier, G.; Andraud, C.; Wang, I.; Bouriau, M.; Baldeck, P. L. *Synth. Met.* **2003**, *138*, 353.
(12) Carrone, G.; Etchenique, R. *Anal. Chem.* **2015**, *87* (8), 4363−4369.
(13) Pettit, D. L.; Wang, S. S.; Gee, K. R.; Augustine, G. J. *Neuron* **1997**, *19*, 465−471.
(14) Chen, W. *J. Nanosci. Nanotechnol.* **2008**, *8* (3), 1019−1051.
(15) Petryayeva, E.; Algar, W. R.; Medintz, I. L. *Appl. Spectrosc.* **2013**, *67* (3), 215−252.
(16) Yi, G.; Sun, B.; Yang, F.; Chen, D.; Zhou, Y.; Cheng, J. *Chem. Mater.* **2002**, *14*, 2910−2914.



DOI: 10.1021/acs.analchem.5b04485
*Anal. Chem.* 2016, 88, 1468−1475

(17) Suyver, J. F.; Aebischer, A.; Biner, D.; Gerner, P.; Grimm, J.; Heer, S.; Kramer, W.; Reinhard, C.; Gudel, H. U. *Opt. Mater.* **2005**, *27*, 1111−1130.
(18) Cheng, Z.; Lin, J. *Macromol. Rapid Commun.* **2015**, *36*, 790−827.
(19) Araya, R.; Andino-Pavlovsky, V.; Yuste, R.; Etchenique, R. *ACS Chem. Neurosci.* **2013**, *4*, 1163−1167.
(20) Filevich, O.; García-Acosta, B.; Etchenique, R. *Photchem.Photobiol.Sci.* **2012**, *11*, 843−847.
(21) Garner, R. N.; Gallucci, J. C.; Dunbar, K. R.; Turro, C. *Inorg. Chem.* **2011**, *50* (19), 9213−9215.
(22) Bahreman, A.; Cuello-Garibo, J. A.; Bonnet, S. *Dalton Trans.* **2014**, *43*, 4494−4505.
(23) He, S. Q.; Krippes, K.; Ritz, S.; Chen, Z. J.; Best, A.; Butt, H. J.; Mailander, V.; Wu, S. *Chem. Commun.* **2015**, *51*, 431−434.
(24) Chen, Z.; Sun, W.; Butt, H. J.; Wu, S. *Chem. - Eur. J.* **2015**, *21*, 9165−9170.
(25) Chen, Z. J.; He, S. Q.; Butt, H. J.; Wu, S. *Adv. Mater.* **2015**, *27*, 2203.
(26) Gainer, C. F.; Utzinger, U.; Romanowski, M. *J. Biomed. Opt.* **2012**, *17*, 076003.
(27) Kowalska, D.; Haro-González, P.; Martín, I. R.; Cáceres, J. M. *Appl. Phys. A: Mater. Sci. Process.* **2010**, *99*, 771−776.
(28) Gamelin, D. R.; Gudel, H. U. *Top. Curr. Chem.* **2001**, *214*, 1−56.
(29) Yu, M.; Li, F.; Chen, Z.; Hu, H.; Zhan, C.; Yang, H.; Huang, C. *Anal. Chem.* **2009**, *81*, 930−935.
(30) Pichaandi, J.; Boyer, J. C.; Delaney, K. R.; van Veggel, F. C. J. M. *J. Phys. Chem. C* **2011**, *115* (39), 19054−19064.
(31) Nadort, A.; Sreenivasan, V. K. A.; Song, Z.; Grebenik, E. A.; Nechaev, A. V.; Semchishen, V. A.; Panchenko, V. Y.; Zvyagin, A. V. *PLoS One* **2013**, *8* (5), e63292.
(32) Larson, D. R.; Zipfel, W. R.; Williams, R. M.; Clark, S. W.; Bruchez, M. P.; Wise, F. W.; Webb, W. W. *Science* **2003**, *300*, 1434−1436.
(33) Wu, S.; Butt, H.-J. *Adv. Mater.* **2015**, DOI: 10.1002/adma.201502843.



DOI: 10.1021/acs.analchem.5b04485
*Anal. Chem.* 2016, 88, 1468−1475